


In vivo deglycosylation of recombinant glycoproteins in tobacco BY-2 cells

Xavier Herman¹ , Johann Far², Marie Peeters¹, Loïc Quinton², François Chaumont^{1,*} and Catherine Navarre¹

¹Louvain Institute of Biomolecular Science and Technology, UCLouvain, Louvain-la-Neuve, Belgium

²Mass Spectrometry Laboratory-MoSys Research Unit, ULiège, Liège, Belgium

Received 18 November 2022;

revised 21 March 2023;

accepted 29 April 2023.

*Correspondence (Tel +32-10-478485; fax

+32-10-473872; email

francois.chaumont@uclouvain.be)

Summary

Production of recombinant pharmaceutical glycoproteins has been carried out in multiple expression systems. However, *N*-glycosylation, which increases heterogeneity and raises safety concerns due to the presence of non-human residues, is usually not controlled. The presence and composition of *N*-glycans are also susceptible to affect protein stability, function and immunogenicity. To tackle these issues, we are developing glycoengineered *Nicotiana tabacum* Bright Yellow-2 (BY-2) cell lines through knock out and ectopic expression of genes involved in the *N*-glycosylation pathway. Here, we report on the generation of BY-2 cell lines producing deglycosylated proteins. To this end, endoglycosidase T was co-expressed with an immunoglobulin G or glycoprotein B of human cytomegalovirus in BY-2 cell lines producing only high mannose *N*-glycans. Endoglycosidase T cleaves high mannose *N*-glycans to generate single, asparagine-linked, *N*-acetylglucosamine residues. The *N*-glycosylation profile of the secreted antibody was determined by mass spectrometry analysis. More than 90% of the *N*-glycans at the conserved Asn297 site were deglycosylated. Likewise, extensive deglycosylation of glycoprotein B, which possesses 18 *N*-glycosylation sites, was observed. *N*-glycan composition of gB glycovariants was assessed by *in vitro* enzymatic mobility shift assay and proven to be consistent with the expected glycoforms. Comparison of IgG glycovariants by differential scanning fluorimetry revealed a significant impact of the *N*-glycosylation pattern on the thermal stability. Production of deglycosylated pharmaceutical proteins in BY-2 cells expands the set of glycoengineered BY-2 cell lines.

Keywords: antibodies, deglycosylation, HCMV gB, molecular farming, *N*-glycosylation, tobacco BY-2 cells.

Introduction

N-glycosylation is one of the most important, complex and ubiquitous post-translational modifications in eukaryotic cells. The presence and composition of *N*-glycans strongly affect protein folding, stability, function and immunogenicity (Nagashima *et al.*, 2018). Post-translational modifications such as *N*-glycosylation are poorly controlled in most recombinant protein expression systems. As a result, the produced glycoproteins are usually characterized by a massive heterogeneity, impairing the control of batch-to-batch reproducibility (Planinc *et al.*, 2017). Moreover, since the different protein glycoforms do not share exactly the same properties, this heterogeneity prevents harnessing the full potential of the product. This is especially the case for therapeutic or vaccine glycoproteins, which differ in terms of activity or immunogenicity depending on the type of *N*-glycan structures present on key *N*-glycosylation sites. The presence of host-specific non-human residues also raises a concern for unwanted immune response. *N*-glycoengineering strategies have been implemented in protein expression systems to redirect the endogenous *N*-glycosylation pathway towards the production of customized *N*-glycan structures. In plants, successful modification of *N*-glycosylation has been obtained in various species (Strasser, 2022).

The first licensed biotherapeutic obtained by molecular farming is a human glucocerebrosidase for Gaucher disease treatment expressed in carrot cells and approved by US FDA under the name of Elelyso™ (Fox, 2012). Recently, a virus-like particle-based vaccine against SARS-CoV-2 produced by agroinfiltration of *Nicotiana benthamiana* plants has been authorized by Health Canada (Medicago Inc., Quebec City, Canada). Transient expression in *N. benthamiana* leaves is the leading production platform in plants but cell cultures such as *Nicotiana tabacum* Bright Yellow-2 (BY-2) offer several advantages that should be considered when selecting an expression system for a particular recombinant protein. First, plant cell lines can be cultivated in bioreactors. Additionally, the glycoproteins of interest might be secreted directly in the culture medium, simplifying the downstream purification process in comparison with crude plant tissues extracts. They are also more amenable to *N*-glycoengineering because modification of the *N*-glycosylation pathway can affect plant development (Fanata *et al.*, 2013; Kaulfürst-Soboll *et al.*, 2021). The BY-2 cell *N*-glycosylation pathway was successfully engineered to suppress the non-human β 1,2-xylose and α 1,3-fucose residues (Hanania *et al.*, 2017; Mercx *et al.*, 2017; Yin *et al.*, 2011). Addition of the human β 1,4-galactose residues (Fujiyama *et al.*, 2007; Misaki *et al.*, 2003; Navarre *et al.*, 2017; Palacpac *et al.*, 1999) and bisecting *N*-

Please cite this article as: Herman, X., Far, J., Peeters, M., Quinton, L., Chaumont, F. and Navarre, C. (2023) *In vivo* deglycosylation of recombinant glycoproteins in tobacco BY-2 cells. *Plant Biotechnol. J.*, <https://doi.org/10.1111/pbi.14074>.

2 Xavier Herman et al.

acetylglucosamine (GlcNAc) (Karg *et al.*, 2010) on recombinant glycoproteins were also demonstrated. Proof of concept that sialylated glycoproteins can be produced in BY-2 cells was provided (Kajiura *et al.*, 2011; Misaki *et al.*, 2006; Paccalet *et al.*, 2007). Recently, a BY-2 cell line lacking complex and hybrid *N*-glycans was generated by inactivation of *N*-acetylglucosaminyltransferases I (GnTI) (Herman *et al.*, 2021). However, a very low α 1,3-fucose signal was still detected by Western blotting (but not mass spectrometry) in *GnTI*-KO lines. The combined inactivation of GnTI and α 1,3-fucosyltransferases (FucT) generated *GnTI/FucT*-KO cell lines, totally devoid of α 1,3-fucose. These strategies are complementary and rely on the knock in or knock down/out of specific glycosyltransferases to redirect the plant *N*-glycosylation machinery towards particular *N*-glycan structures.

While glycosylation is a critical feature for some recombinant glycoproteins, the presence of *N*-glycans might be dispensable for others. Proteins whose properties are not significantly affected by the presence of *N*-glycans could benefit from a glycosylation shortening strategy. Indeed, the removal of *N*-glycans suppresses non-human residues, increases homogeneity and simplifies downstream processing (Van Landuyt *et al.*, 2019). In addition, the absence of *N*-glycan structures can confer useful properties to the glycoprotein, even if the native form is glycosylated. For example, immunoglobulins G (IgGs) carry an *N*-glycan attached to the conserved Asn297 residue in the constant domain 2 (CH2) of both heavy chains from the crystallizable fragment (Fc), which is essential for Fc effector functions (Kiyoshi *et al.*, 2017). Besides the gain in homogeneity, deglycosylated IgGs can be desirable for applications that do not require Fc effector functions because these can cause undesired inflammation and cytotoxicity (Ju and Jung, 2014). Moreover, deglycosylated IgGs are a promising class of therapeutics for autoimmune diseases because they display a dominant suppressive effect on immune complex-mediated inflammation (Nandakumar *et al.*, 2013). Non-glycosylated IgGs can also be useful in diagnostic procedures such as *in vitro* immunoassays since Fc glycosylation might interfere with the detection of aberrant glycoforms of a disease biomarker (Lee *et al.*, 2020). Additionally, vaccine antigens can benefit from the suppression of large *N*-glycans. Indeed, viral surface proteins are often highly glycosylated, facilitating immune evasion by shielding specific epitopes (Huang *et al.*, 2022). Mice immunization studies evaluating the potential of viral antigens with shortened (or no) *N*-glycosylation showed promising results. *In vitro* deglycosylated influenza hemagglutinin elicits higher cross-strain immune responses, stronger neutralization, and higher protective effect than the fully glycosylated form produced in HEK 293 (Chen *et al.*, 2014a; Wang *et al.*, 2009). Partially deglycosylated SARS-CoV spike protein receptor binding domain elicits stronger specific antibody responses and a higher level of neutralizing antibodies (Chen *et al.*, 2014b). Deglycosylation of SARS-CoV-2 spike protein also results in stronger immune responses as well as better and broader protection against variants of concern (Huang *et al.*, 2022; Wu *et al.*, 2022).

In vitro enzymatic deglycosylation is a relevant strategy to produce deglycosylated proteins for small-scale studies but this is not suitable for industrial production. Recombinant glycoproteins can rather be deglycosylated *in vivo*. Transient co-expression in *N. benthamiana* leaves of *Flaviobacterium meningosepticum* peptide:*N*-glycosidase F (PNGase F) with antibodies or antigenic

proteins resulted in the production of deglycosylated recombinant proteins (Mamedov *et al.*, 2012). However, due to the PNGase F substrate specificity (*N*-glycans without core α 1,3-fucose residues), PNGase F and the recombinant proteins had to be fused with the KDEL endoplasmic reticulum (ER) retention sequence to avoid formation of complex *N*-glycans that would be PNGase F-resistant. Besides the impact on protein accumulation and storage, the drawback of this strategy is that PNGase F deaminates the Asn residue to Asp, hence modifying the peptide sequences. Later, protein antigens were transiently co-expressed with endo- β -*N*-acetylglucosaminidase H (EndoH) from *Streptomyces plicatus* in *N. benthamiana* leaves (Mamedov *et al.*, 2017, 2021). EndoH hydrolyzes the *N*-acetylglucosamine (GlcNAc)-GlcNAc bound of high mannose *N*-glycans, leaving a single GlcNAc on the Asn residue, which might be important to maintain the overall protein fold. However, EndoH substrate specificity required the retention of all recombinant proteins in the ER.

To circumvent the limitation of fusing the C-terminus of proteins with an ER-retention signal, it was proposed to express an endo- β -*N*-acetylglucosaminidase in complex glycan-deficient hosts. This strategy was first achieved by expressing endo- β -*N*-acetylglucosaminidase T (EndoT) from the fungus *Hypocrea jecorina*, which displays similar substrate specificity as EndoH, in the *GnTI*-inactivated human embryonic kidney (HEK 293S*GnTI* (-)) cell line producing only high mannose *N*-glycans (Meuris *et al.*, 2014). This system is called GlycoDelete®. *N*-glycans of the GlycoDelete cell line were shortened down to a single GlcNAc, which can be further galactosylated and sialylated, resulting in the production of recombinant glycoproteins with nearly uniform, small *N*-glycans. This elegant and effective GlycoDelete strategy was then successfully implemented in an *Arabidopsis thaliana complex glycan less 1 (cgl1)* mutant lacking GnTI activity (Piron *et al.*, 2015). The GlycoDelete *A. thaliana* plant was obtained by expressing EndoT specifically in the seeds, thus allowing convenient accumulation and storage of recombinant proteins without impacting plant growth. EndoT was targeted to the medial Golgi membrane by fusing its catalytic region with the cytoplasmic, transmembrane, and stem domains of At β 1,2-xylosyltransferase (XylT). Expression of activation associated secretory protein 1 (ASP1) from helminth in the seeds of the GlycoDelete plant showed that the two ASP1 *N*-sites were completely trimmed to a single GlcNAc (Piron *et al.*, 2015). The GlycoDelete technology was also validated in the yeast *Pichia pastoris* (Wang *et al.*, 2020), the filamentous fungus *Aspergillus oryzae* (Li *et al.*, 2020) and CHO cells (Kang *et al.*, 2022).

Here, we used the GlycoDelete strategy to produce deglycosylated human IgG and viral envelope glycoprotein B (gB) ectodomain from the human cytomegalovirus (HCMV) in transgenic BY-2 cells. The latter contains 18 *N*-glycosylation sites and is a potential candidate for a recombinant vaccine against HCMV (Schleiss *et al.*, 2017). To do so, the *GnTI*-KO and *GnTI/FucT*-KO lines, producing glycoproteins bearing only oligomannose-type *N*-glycans, were transformed with T-DNAs containing both EndoT and the recombinant glycoprotein expression cassettes. The *XylT/FucT*-KO BY-2 cell line (Mercx *et al.*, 2017) was also used to produce humanized recombinant glycoproteins. The glycosylation status of the glycoproteins was confirmed by *in vitro* enzymatic assays and mass spectrometry identification of the *N*-glycans. We also investigated the influence of the glycan alteration on the thermal stability of IgGs by differential scanning fluorimetry.

Results

AtXylT-EndoT is localized in the Golgi apparatus and propeptide-processed in BY-2 cells

The N-terminal signal sequence of EndoT was swapped for the *medial*-Golgi targeting signal of AtXylT as proposed by Piron *et al.* (2015). The sequence encoding the N- and C-terminal propeptides of EndoT were included in the construct (Figure 1a). This chimeric *EndoT* gene was driven by the enhanced CaMV 35S promoter and cloned into a pPZP-*hpt* binary vector to obtain transgenic BY-2 cells. In addition, to confirm the localization of EndoT in the Golgi apparatus, the chimeric EndoT was fused to the Venus fluorescent protein at C-terminus.

EndoT-Venus cell lines were imaged by confocal microscopy and the Venus signal was detected in typical Golgi-like mobile vesicles localized near the plasma membrane and nucleus as well as in transvacuolar cytoplasmic strands (Figure 1b, Movie S1), suggesting that EndoT-Venus is efficiently targeted to the Golgi stacks thanks to the transmembrane of AtXylT.

The distribution of EndoT in *EndoT*- and *EndoT-Venus*-expressing cell lines was then investigated by Western blotting using anti-EndoT antibodies (Figure 1c). In the microsomal fractions, bands corresponding to EndoT-Venus and EndoT were detected at around 70 and 43 kDa, respectively, corresponding to the molecular mass of the full-length, unprocessed proteins. A band around 32 kDa was also detected in the total soluble cellular proteins (TSCP) and culture medium (CM) of both lines. Since EndoT and EndoT-Venus contained N- and C-terminal endogenous propeptides, processing of the precursor in BY-2

cells can be expected. This would release soluble EndoT in the Golgi lumen and, eventually, in the CM.

N-glycan composition of *GnTI*-KO and *GnTII/FucT*-KO BY-2 cell lines is suitable for EndoT processing

EndoT has a specific activity towards high mannose *N*-glycans. As a result, to generate mono-GlcNAc proteins, this enzyme had to be expressed in a BY-2 cell line devoid of complex *N*-glycans. Such BY-2 cell lines were previously obtained by knocking out *GnTI* as well as *GnTI* and *FucT* glycosyltransferase genes and mass spectrometry analysis of secreted glycoproteins from one line of each cell type showed a similar *N*-glycan composition (Herman *et al.*, 2021). To investigate the reproducibility of the *N*-glycan content in several independent transgenic cell lines, four *GnTI*-KO and three *GnTII/FucT*-KO cell lines were grown in D11b production medium, which was optimized for the accumulation of antibodies in BY-2 cells (Vasilev *et al.*, 2013). The secreted glycoproteins were analysed by MALDI FT-ICR mass spectrometry (Figure S1). A highly reproducible and similar *N*-glycome was obtained for both *GnTI*-KO and *GnTII/FucT*-KO cell lines, with mainly Man5 (87% and 89%, respectively) and Man4 (9% and 7%, respectively) structures. The remaining structures were all oligomannosidic structures (Man3-9). The *N*-glycan distribution obtained from the *GnTI*-KO cell lines grown in Murashige and Skoog medium (MS) (Figure S1) was very similar to that observed for D11b cultures, with mainly Man5 (80%) and Man4 (14%) glycans. No α 1,3-fucosylated *N*-glycan structure was detected in *GnTI*-KO cell lines. Hence, we concluded that *N*-glycans found on secreted glycoproteins of *GnTI*-KO and *GnTII/FucT*-KO cell lines grown in either MS or D11b media are suitable for EndoT processing.

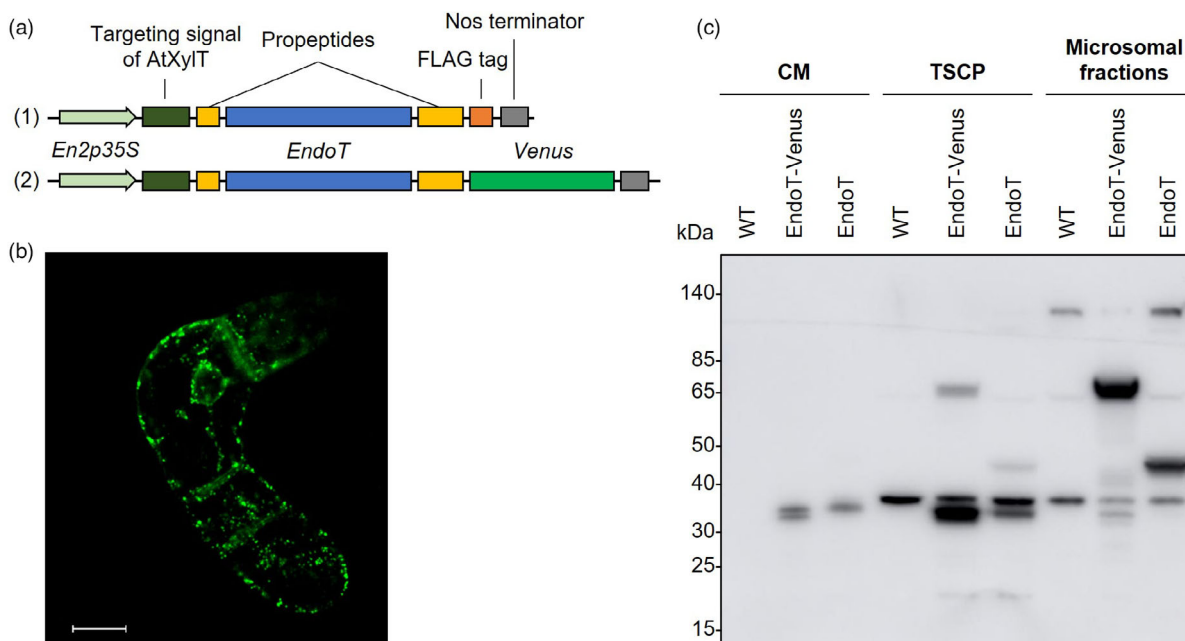


Figure 1 Localization of AtXylT-EndoT and *in vivo* processing in BY-2 cells. (a) Schematic representation of AtXylT-EndoT (1) and AtXylT-EndoT-Venus (2) expression cassettes. (b) Localization of EndoT-Venus fused to the signal-anchor of *A. thaliana* β 1,2-xylosyltransferase. λ_{exc} : 514 nm; λ_{em} : 537 nm. Scale bar: 20 μ m. The same parameters were used for Movie S1 (c) 35 μ L of 7-day-old culture medium (CM), 35 μ g of total soluble cellular proteins (TSCP) and microsomal fractions from wild type (WT), EndoT and EndoT-Venus BY-2 cell cultures were analysed by Western blotting using an anti-EndoT serum and a horseradish peroxidase-linked secondary antibody. Hollow (○) and full (●) dots indicate bands, the size of which correspond to unprocessed EndoT-Venus and EndoT, respectively, whereas a star (*) indicates processed EndoT and EndoT-Venus. Diamond (◇) mark signals from endogenous proteins of BY-2 cells.

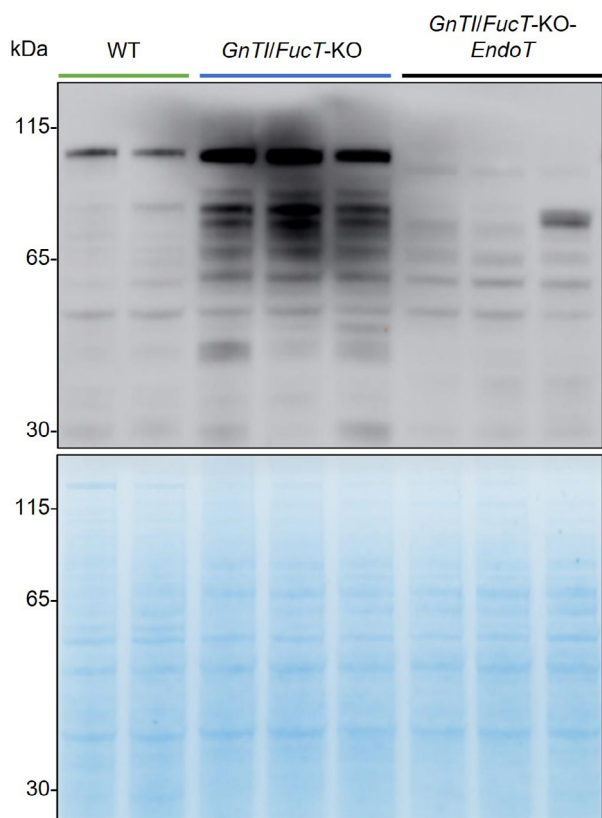


Figure 2 Deglycosylation of endogenous glycoproteins by EndoT. 25 μ g of TSCP from WT cell lines (lane 1: WT-gB 23, lane 2: WT), *GnTI/FucT-KO* cell lines (*GnTI/FucT-KO*-gB #1, 5 and 16) and *GnTI/FucT-KO-EndoT* cell lines (*GnTI/FucT-KO-EndoT*-gB #19, 29, 30) were analysed by Western blotting using concanavalin A coupled to horseradish peroxidase. A colloidal blue gel is displayed as a loading control.

Expression of EndoT strongly reduces *N*-glycosylation

The *N*-glycans decorating cellular glycoproteins from WT, *GnTI/FucT-KO* and *GnTI/FucT-KO-EndoT* cell lines were compared by Western blot analysis using the lectin concanavalin A, which binds high mannose *N*-glycans (Figure 2). The low signal observed in WT samples correlates with the presence of only 20% of high mannose *N*-glycans in the cellular proteins (Hanania *et al.*, 2017). The signals obtained for the *GnTI/FucT-KO* cell lines agree with the high proportion of high mannose *N*-glycans. On the contrary, the reduction of the signal observed in *GnTI/FucT-KO-EndoT* cell lines suggests that a large part of the high mannose *N*-glycans was processed by EndoT. The reduction was estimated at ~75% by semi-quantitative analysis of Western blot signals.

N-glycosylation engineering negatively affect the growth kinetics of BY-2 cell lines

The impact of *GnTI* inactivation and *EndoT* expression on cell growth kinetics was explored in MS medium (Figure S2). Depletion of complex *N*-glycans led to a slower growth (detectable already from day 4), resulting in a 11% drop in maximal fresh weight (FW) at day 7. Expression of EndoT in high mannose cell lines seems to further reduce the growth rate with a stronger drop (29.5% as compared to WT cell lines) of maximal FW. Furthermore, while cell density is stable after day 7 for WT

cell lines, it drops for high mannose cell lines (–12%) and EndoT-expressing lines (–34%).

Human IgG is successfully expressed by and purified from glyco-engineered cell lines

The following lines were obtained: WT, *XyII/FucT-KO*, *GnTI-KO* and *GnTI/FucT-KO* cell lines expressing the human immunoglobulin 2 (IgG2) anti-IgM Lo-BM2; *GnTI-KO* and *GnTI/FucT-KO* cell lines co-expressing IgG2 and EndoT. To select elite cell lines, IgG2 accumulation in the CM and EndoT signal in the total cellular proteins (TCP) were assessed by Western blotting (Figure S3). EndoT could be detected in most *GnTI-KO-EndoT-IgG2* and *GnTI/FucT-KO-EndoT-IgG2* cell lines, with sizes corresponding to full-length (~43 kDa) and propeptide-processed (~32 kDa) proteins. From now on, IgG2 glycovariants will be named according to their main *N*-glycan structure: IgG2_{FG} for fully glycosylated (WT-IgG2); IgG2_{ΔX/ΔF} for xylose/α1,3-fucose-deleted (*XyII/FucT-KO-IgG2*); IgG2_{HM} for high mannose (*GnTI-KO-IgG2* and *GnTI/FucT-KO-IgG2*) and IgG2_{MG} for mono-GlcNAc (*GnTI-KO-EndoT-IgG2* and *GnTI/FucT-KO-EndoT-IgG2*). Cell lines, major expected *N*-glycan structure and glycovariants are summarized in Table S1.

To monitor IgG2 accumulation in the CM, the cell line *GnTI/FucT-KO-IgG2* #17 was grown in MS or D11b medium and the CM was analysed by Western blotting (Figure S4a). Intact IgG2_{HM} was already detected after 5 days of culture and the signal culminated at day 7 or 10 in D11b medium. IgG2_{HM} and IgG2_{MG} concentrations in D11b 10-day-old CM were quantified by ELISA in six independent transgenic lines for each glycovariant (IgG2_{HM} or IgG2_{MG}) between 10 and 45 mg/L (Table S2a). These values were similar to the concentrations described for IgG2 expressed in BY-2 wild type (10–40 mg/L) by Magy *et al.* (2014). Since ELISA plates were coated with human IgMs, this confirmed that IgG2_{HM} and IgG2_{MG} were able to bind the antigen. To compare the *N*-glycosylation status of the heavy chain, CM containing IgG2_{HM} or IgG2_{MG} were run on the same gel in reducing conditions, with and without prior EndoH and PNGase F *in vitro* deglycosylation treatment (Figure S5a). PNGase F cleaves *N*-glycans that are not α1,3-fucosylated. EndoH cleaves high mannose *N*-glycans to produce mono-GlcNAc *N*-glycosylated asparagines. Accordingly, the size shift resulting from *in vitro* deglycosylation by EndoH or PNGase F was clearly detectable for IgG2_{HM} but not for IgG2_{MG}, confirming the high mannose *N*-glycan type of IgG2_{HM} and the *in vivo* deglycosylation of IgG2_{MG}.

The IgG2 glycovariants were then purified through protein A affinity chromatography and analysed by SDS-PAGE (Figure S6a). One sample was analysed in reducing conditions to confirm the correct assembly of heavy and light chains (Figure S6b). The purity of IgG2 was also tested by size exclusion chromatography (Figure S6c) followed by SDS-PAGE and Western blotting (Figure S6d). Both IgG2_{HM} and IgG2_{MG} eluted in a single peak (fractions 11 and 12). IgG2_{MG} is eluted slightly earlier than IgG2_{HM}, which was expected since the molecular hydrodynamic radius is reported to increase after Fc deglycosylation (Zheng *et al.*, 2011). The quantity of purified IgG2, starting from 150 mL CM and measured by RC-DC assay, reached up to 3 mg.

Glyco-engineering strategies confer the expected *N*-glycosylation profile to IgG glycovariants

The glycosylation profile of purified IgG2 was then analysed by liquid chromatography followed by tandem quadrupole orbitrap mass spectrometry (LC–MS/MS). *N*-glycans detected on the conserved *N*-site EEQFN*STFR of the heavy chain CH2 domain

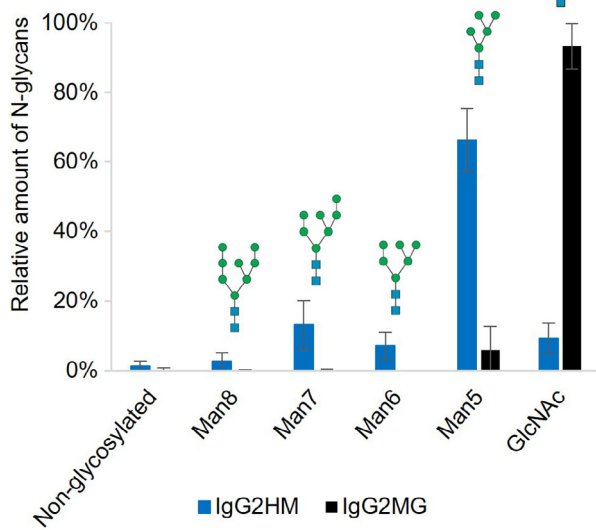


Figure 3 Relative amount of N-glycans on the N-site EEQFN*STFR of secreted IgG2. N-glycosylation was determined by LC-MS/MS of IgG2 samples purified from 10 days-old D11b culture medium. Error bars represent standard deviation of $n = 5$ (IgG2HM: GnTI-KO-IgG2 #12, 25, 30, GnTI/FucTKO-IgG2 #17, 20) and $n = 4$ (IgG2MG: GnTI-KO-EndoT-IgG2 #9, 12; GnTI/FucT-KO-EndoT-IgG2 #6, 16) independent cell lines. Structures accounting for <1% of N-glycans were not represented.

are summarized in Figure 3 and Table S3. No α 1,3-fucose-containing N-glycans were detected in GnTI-KO cell lines. The EEQFN*STFR site had a N-glycosylation occupancy of 98.7% for IgG2_{HM} and 99.7% for IgG2_{MG}. As anticipated, N-glycan diversity was low for IgG2_{HM} and IgG2_{MG}, with only five and two different N-glycan structures detected at more than 1%, respectively. Man5 was the main structure detected for IgG2_{HM}, accounting for 66% of CH2 N-glycans. The majority of N-glycans detected for IgG2_{MG} (93%) were trimmed down to mono-GlcNAc structures, indicating a highly efficient *in vivo* processing by EndoT. The remaining structures identified were mainly Man5 (6%), along with traces of other oligomannosidic structures.

Besides the conserved EEQFN*STFR N-site in the CH2 domain, the variable region of the Lo-BM2 heavy chain contained the predicted N-glycosylation site CVRPN*YSGF. It displayed a much lower occupancy rate with only 9% and 11% for IgG2_{HM} and IgG2_{MG}, respectively (Figure S7a, Table S3). N-glycans observed at this site were mostly Man5 for both IgG2_{HM} and IgG2_{MG} (89% and 70% of the glycosylated forms, respectively). A small proportion of mono-GlcNAc structures could be detected on IgG2_{MG} (23% of the glycosylated forms) but not on IgG2_{HM}.

Intriguingly, a third N-glycosylation site was also identified on the non-canonical N-site (TVSWN*SGAL) with a significant occupation rate of 13% (Figure S7b, Table S3). Similar to the two other N-sites of IgG2_{HM}, the main structure identified was Man5.

N-glycosylation was similar in GnTI-KO and GnTI/FucT-KO backgrounds (Figure S8).

Glycovariants display different thermal stability

Having an antibody with various N-glycosylation profiles allowed us to question the effect of this glycosylation on the stability of the protein. A differential scanning fluorimetry (DSF) assay, also

called thermal shift assay, was carried out to compare the thermal stability of the different IgG2 glycovariants. Besides the IgG2_{FG}, IgG2_{ΔX/ΔF}, IgG2_{HM} and IgG2_{MG} produced in this study, IgG2_{FG} and IgG2_{ΔX/ΔF} previously purified from independent transgenic cell lines (Magy *et al.*, 2014; Mercx *et al.*, 2017) were also analysed. The melting temperature (T_m) was calculated based on the first derivative of the melting curves (Figure S9a,b). DSF assay with new and old IgG2_{FG} and IgG2_{ΔX/ΔF} samples gave similar results, thereby confirming the robustness of the BY-2 production platform (Figure S10). The lowest T_m , 60.5 °C, was obtained for IgG2_{FG} while the highest T_m , 66.9 °C, was observed for IgG2_{ΔX/ΔF} (Figure 4a). IgG2_{HM} and IgG2_{MG} resulted in intermediate T_m of 63.4 °C and 61.9 °C, respectively. A drastic increase in thermal stability (+6.4 °C) was thus observed when comparing IgG2_{FG} and IgG2_{ΔX/ΔF}, demonstrating that core- α 1,3-fucosylation and/or β 1,2-xylosylation impact thermal stability of the IgG2. The effect of N-glycans on the thermal stability of IgG1 was also assessed, using hlgG1 Lo-BM2 produced in WT and XylTI/FucT-KO BY-2 cells. The respective DSF T_m , 62.1 °C (IgG1_{FG}) and 70.1 °C (IgG1_{ΔX/ΔF}), were consistent with those obtained for IgG2 (Figures 4b, S9b,c). IgG1 accumulation in CM is reported in Table S2b.

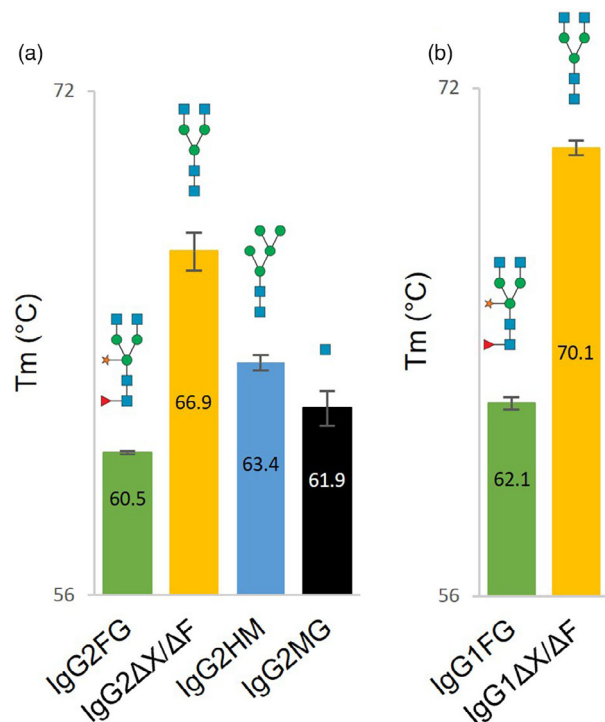


Figure 4 Thermal stability of IgG glycovariants. a. T_m of IgG2 glycovariants secreted in BY-2 CM measured by differential scanning fluorimetry analysis. b. T_m of IgG1 glycovariants secreted in BY-2 CM measured by DSF analysis. IgG were purified from two (IgG2_{FG}), two (IgG2_{ΔX/ΔF}), six (IgG2_{HM}), three (IgG2_{MG}), two (IgG1_{FG}) and four (IgG1_{ΔX/ΔF}) independent cell lines and $n = 6$ for technical replicates. T_m was obtained as the mean of the T_m calculated for each independent sample. Error bars represent standard deviation of the mean T_m obtained for the independent cell lines. As an indication, the main N-glycan structure of each glycovariant at the CH2 N-site is represented above the corresponding bar. IgG1 N-glycans are the expected structures based on IgG2, it was not analysed by MS.

Glycovariants of glycoprotein B from HCMV display different electrophoretic sizes

The gB ectodomain was already successfully produced as a secreted glycoprotein containing both complex and high mannose structures (gB_{FG}) in WT BY-2 cells (Smargiasso *et al.*, 2019). Due to the 18 *N*-glycosylation sites in the gB ectodomain, it was produced as a population of glycoforms characterized by a huge meta-, macro and micro-heterogeneity (variations of glycan structures across multiple sites of a protein, occupancy and variation of glycans at a given site, respectively (Čaval *et al.*, 2021)).

Here, a version of gB devoid of β 1,2-xylose and α 1,3-fucose (gB _{Δ X/ Δ F}) was obtained in the *XylTII/FucT*-KO cell line. We also produced gB in *GnTI*-KO and *GnTII/FucT*-KO cell lines (gB_{HM}). Expression of gB in TSCP of those cell lines was analysed by Western blotting (Figure 5a). gB_{HM} was detected both as an intact protein at ~100–105 kDa and degradation fragments, mainly at 25–30 kDa. Intact gB_{HM} was slightly smaller than gB_{FG} and gB _{Δ X/ Δ F}. This variation in size likely resulted from differences in *N*-glycan composition.

Next, the gB ectodomain was co-produced with EndoT in the *GnTII/FucT*-KO cell line (gB_{MG}). TCP and TSCP from *GnTII/FucT*-KO-*EndoT*-gB cell lines were analysed by Western blotting using antibodies against gB or EndoT (Figure 5b,c, respectively). gB was detected in most transgenic lines (#17, 18, 19, 23, 25, 29, 30, 33,

34) (Figure 5b). EndoT-specific signal was observed, but only for some transgenic cell lines (#19, 29, 30, 34) (Figure 5c). The bands corresponding to intact gB showed distinct patterns according to the cell lines. In cell lines without EndoT production, the migration behaviour was similar to gB_{HM} (#17, 18, 23, 25, 33), while in EndoT-expressing cell lines (#19, 29, 30, 34), the bands corresponding to intact gB_{MG} displayed a remarkably shifted mobility in regard to gB_{HM}. This mobility shift was attributed to the *in vivo* processing of high mannose *N*-glycans decorating gB by EndoT. It was observed as a smear lower than gB_{HM}, compatible with processed glycosylated gB subjected to various levels of *N*-glycan truncation.

To monitor gB_{HM} accumulation in the CM, two *GnTI*-KO-gB (#2, 4) and two *GnTII/FucT*-KO-gB (#5, 16) cell lines were grown in D11b medium (Figure 5d). Intact gB_{HM} was already detected after 4 days of culture and the signal culminated at day 7 or 10. Accumulation of secreted gB in *GnTII/FucT*-KO-*EndoT*-gB CM was also investigated by Western blotting, both in MS and D11b media, after 5, 7, 10 and 13 days of culture (Figure 5b). However, no intact gB_{MG} could be detected although gB_{MG} degradation fragments were observed in higher amount than in the control *GnTII/FucT*-KO-gB #5 line, suggesting that gB_{MG} was either less stable than gB_{HM} or more subject to protease-mediated proteolysis. Finally, gB_{HM} and gB_{MG} concentrations in 10-day-old D11b CM were measured by ELISA and reached up to 44 mg/L and 45 mg/L, respectively (Table S2c). Although degradation

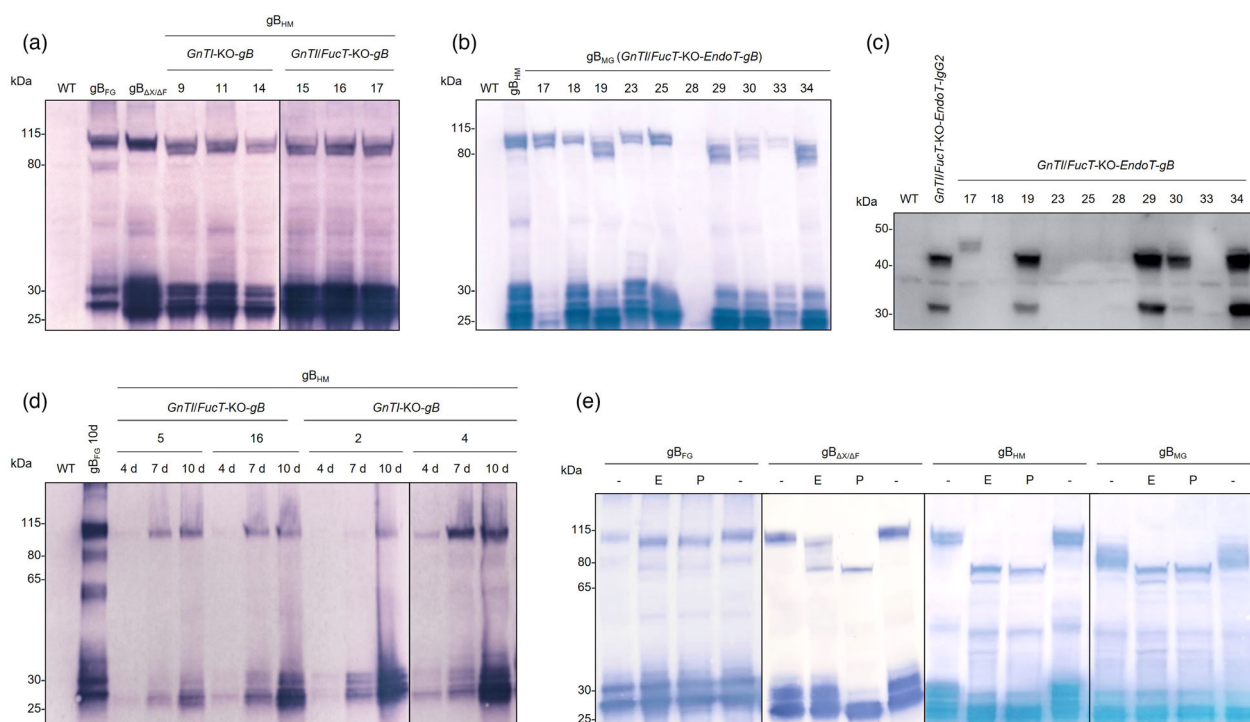


Figure 5 Expression of gB HCMV in glyco-engineered BY-2 cell lines. Twenty μ g of TSCP from *GnTI*-KO-gB and *GnTII/FucT*-KO-gB cell lines (a) and *GnTII/FucT*-KO-*EndoT*-gB (b) cell lines and indicated controls were analysed by Western blotting using antibodies raised against gB and AP-coupled secondary antibodies. Signal was detected using a precipitating substrate. gB_{FG} from WT-gB cell line is displayed as a positive control. (c) Twenty μ g of TCPs from *GnTII/FucT*-KO-*EndoT*-gB cell lines and indicated controls were analysed by Western blotting using antibodies raised against EndoT and AP-coupled secondary antibodies. Signal was detected using a chemiluminescent substrate. (d) Accumulation of gB_{HM} in the culture medium of indicated cell lines. Thirty-five μ L of CM from 4, 7 or 10-day-old D11b cultures were analysed by Western blotting using anti-gB antibody and AP-linked secondary antibody. (e) Deglycosylation gel shift assay for gB glycovariants. Immunodetection of gB glycovariants without deglycosylation (–) and after deglycosylation by EndoH (E) or PNGase F (P). Twenty μ g of TSCP from WT-gB #23 (gB_{FG}), *XylTII/FucT*-KO-gB #4 (gB _{Δ X/ Δ F}), *GnTII/FucT*-KO-gB #5 (gB_{HM}), *GnTII/FucT*-KO-*EndoT*-gB #29 (gB_{MG}) cell lines were loaded. Primary and secondary antibodies were anti-gB antibodies and AP-linked antibodies, respectively.

fragments account for a large proportion of the gB produced, the relatively high yield obtained showed that the glyco-engineered BY-2 cell lines were suitable to produce complex recombinant glycoproteins.

Glycoprotein B glycovariants are differentially processed *in vitro* by glycosidases

To further study and compare the *N*-glycosylation profile of gB_{FG}, gB_{ΔX/ΔF}, gB_{HM} and gB_{MG}, an *in vitro* deglycosylation assay was carried out using either PNGase F or EndoH.

TSCPs from WT-gB, *XylII/FucT*-KO-gB, *GnTII/FucT*-KO-gB and *GnTII/FucT*-KO-*EndoT*-gB cell lines were denatured, incubated with PNGase F or EndoH and then resolved by gel electrophoresis and Western blotting (Figure 5e). A slight mobility shift was observed for gB_{FG} after the action of EndoH or PNGase F. This result was expected since complex structures of gB_{FG} contain α1,3-fucose and therefore cannot be processed by EndoH or PNGase F (Smargiasso *et al.*, 2019). The small (but still detectable) mobility shift was therefore related to the processing of the few *N*-glycans that were oligomannosidic (Smargiasso *et al.*, 2019) and were equally cleaved by both glycosidases. EndoH-mediated deglycosylation of gB_{ΔX/ΔF} resulted in an incomplete shift while PNGase F-mediated deglycosylation was compatible with a completely deglycosylated gB (predicted size: 73 kDa), highlighting the presence of non-fucosylated complex *N*-glycans (such as GnGn), which are substrates for PNGase F but not EndoH. Deglycosylation of gB_{HM} with either EndoH or PNGase F both resulted in a large mobility shift compatible with complete deglycosylation. This clearly demonstrates the dramatic increase in high mannose *N*-glycan structures decorating gB_{HM} when produced in *GnTII/FucT*-KO cell lines. Finally, complete deglycosylation of gB_{MG} was also obtained with both EndoH and PNGase F, generating highly similar bands as with gB_{HM}. Deglycosylation assay was also carried out with the CM collected by filtration from *GnTII/FucT*-KO-gB cell cultures. Similar results as the assays using TSCPs were obtained (Figure 55b).

Finally, to investigate the stability and EndoT-mediated processing of gB_{HM} in the CM, gB_{HM}-containing CM was spiked in CM from *GnTII/FucT*-KO and *GnTII/FucT*-KO-*EndoT* cell lines (Figure S11). After 22 h incubation at 25 °C, no change in size nor intensity of gB signal was observed by Western blotting, suggesting that EndoT is poorly active or too diluted in the CM and that most of the degradation occurs either in the secretory pathway or in the apoplast of BY-2 cells.

Discussion

In this study, we generated BY-2 cell lines producing deglycosylated proteins via the expression of EndoT in a high mannose *N*-glycosylation background. The high mannose and deglycosylated cell lines were validated by producing a human IgG2 as well as the ectodomain of the glycoprotein B from HCMV envelope, both reaching up to more than 40 mg/L. Lectin blot analysis, *in vitro* deglycosylation assays and site-specific glycoproteomics confirmed the truncation of *N*-glycans decorating endogenous and recombinant glycoproteins by EndoT. Noticeably, more than 93% of *N*-glycans found at the conserved Asn residue in the CH2 domain of IgG2 were effectively shortened to a single GlcNAc. IgG and gB glycovariants were also successfully obtained using a wild type cell line, a cell line devoid of xylose and α1,3-fucose non-human residues (*XylII/FucT*-KO) and high mannose cell lines (*GnTII*-KO and *GnTII/FucT*-KO). Mass spectrometry experiments

confirmed the expected *N*-glycosylation profiles and revealed a high reproducibility. Besides the interest of controlling the type of *N*-glycan present on recombinant proteins to tune their properties, reproducibility and homogenization of *N*-glycan content are major assets to ease quality control for pharmaceutical proteins.

The comprehensive *N*-glycosylation profile of IgG2 glycovariants was determined by LC/MS–MS. Two *N*-glycosylation sites were predicted based on the consensus N-X-S/T sequence. The glycopeptide EEQFN*STFR in the conserved CH2 domain showed a very high occupancy rate (99%–100%, Figure 3, Table S3). The second putative glycopeptide CVRPN*YSGF located in the variable region of heavy chain, displayed a much lower occupancy rate (9–11%) (Figure S7a, Table S3). This could be related to the presence of a Ser in the +2 position, which was associated with a lower fraction of occupancy than Thr (Kasturi *et al.*, 1995). It could also be linked to an unfavourable amino acid context or steric hindrance. An additional *N*-glycosylation site was detected at the non-canonical sequence TVSWN*SGAL in the conserved CH1 domain of the heavy chain. This atypical N-site had already been reported as a backwards consensus *N*-glycosylation motif (S/T)XN on antibodies from human serum and on human IgG1 and IgG2 produced in CHO and HEK 293 cells (Valliere-Douglass *et al.*, 2009, 2010). The *N*-glycan occupancy level was only 0.5 to 2% as compared to the 13% measured in our study for BY-2-produced IgG2. Detection of this non-canonical *N*-glycosylation site was made possible because of Multi-Enzymatic Limited Digestion (MELD) instead of the classic trypsin-only treatment (that would result in a 58-residue peptide including TVSWN*SGAL). This MELD technique allows generating a more diverse (glyco)peptide library and the exhaustive determination of post-translational modifications.

Analysis of the *N*-glycosylation library found at the CH2 *N*-glycosylation site showed that the glyco-engineered cell lines produced the anticipated glycoforms. The main *N*-glycan found on IgG2_{HM} (Man5) and IgG2_{MG} (mono-GlcNAc) accounted for 66% and 93% of the *N*-glycans, respectively (Figure 3, Table S3). The main *N*-glycan of IgG2_{FG} (GnGnXF) accounted for 74.5% of all *N*-glycans and those of IgG2_{ΔX/ΔF} (GnGn) for 69%, as determined by Navarre *et al.* (2017) and Mercx *et al.* (2017), respectively. Thus, production of an antibody in glycoengineered BY-2 cell lines generates glycovariants with one defined, predominant *N*-glycan structure.

Thermal stability of IgG2 and IgG1 glycovariants was measured by DSF. IgG2 showed a single transition in the DSF graphs while IgG1 displayed two transition peaks. A single transition peak indicates an overlap of the different domain denaturation signals. The presence of two peaks, in contrast, suggests that at least two domains denature at different temperatures. The IgG CH3 domain is reported to unfold at a higher temperature than the CH2 domain (Akazawa-Ogawa *et al.*, 2018; Meuris *et al.*, 2014). Hence, we speculated that the first IgG1 peak could correspond to the CH2 domain while the second one would be for the CH3 domain. This was further confirmed with IgG1_{ΔX/ΔF} by the change in T_m observed for the first peak of IgG1_{FG} and IgG1_{ΔX/ΔF}, while the second T_m was stable around 75 °C (Figure S9). Indeed, the CH2 domain, with the conserved N297, is the most susceptible to be (de)stabilized by glyco-engineering.

Relative CH2 T_m measured for IgG2_{ΔX/ΔF}, IgG2_{HM} and IgG2_{MG} were consistent with those previously reported in the literature by DSF, differential scanning calorimetry and intrinsic fluorescence spectroscopy for IgG1 (Meuris *et al.*, 2014; Wada *et al.*, 2019; Zheng *et al.*, 2011). Indeed, these studies showed that complex

N-glycosylation results in a higher T_m than Man5, which in turn is more stable than the mono-GlcNAc stump. However, to the best of our knowledge, this is the first thermal stability study of an antibody with typical plant *N*-glycans (GnGnXF). IgG2_{FG} displayed the lowest T_m among all glycovariants. To consolidate this observation, DSF was also carried out with IgG1_{FG} and IgG1_{AX/AF} and provided similar results, IgG1_{AX/AF} being significantly more stable than IgG1_{FG} ($\Delta T_m = +8$ °C). This result suggests that the presence of β 1,2-xylose and/or α 1,3-fucose residues triggers a destabilizing effect on IgG2 and IgG1. The presence of typical mammalian core α 1,6-fucose residues slightly increased the stability of most IgG1 glycoforms, as opposed to our findings on IgG_{FG} (Wada *et al.*, 2019). However, the absence of xylose and the difference in fucose linkages should mitigate the comparison with the results obtained for IgG_{FG} and IgG_{AX/AF}. Generation of IgG_{AX} and IgG_{AF} would shed light on the impact of the plant core-fucose linkage (and core-xylose presence) on IgG thermal stability.

The production of a more complex, heavily glycosylated, recombinant glycoprotein in these new cell lines was also evaluated. The ectodomain of gB was chosen because it is a vaccine candidate against HCMV and was already produced in WT BY-2 cells (Smargiasso *et al.*, 2019). The ability to produce gB glycovariants constitutes a powerful tool to study the impact of *N*-glycosylation on immunogenicity and hence develop better vaccines. Interestingly, gB glycovariants showed different electrophoretic mobility on Western blotting: gB_{FG} and gB_{AX/AF} (that lacks β 1,2-xylose and α 1,3-fucose residues) electrophoretic sizes were slightly higher than that of gB_{HM} (probably decorated mainly with Man5), while an important size shift was detected for gB_{MG} (Figure 5a,b,e).

In vitro deglycosylation assay of gB glycovariants was carried out to obtain a global insight in *N*-glycan compositions (Figure 5e). The electrophoretic mobility shifts were consistent with expected gB glycoforms. Particularly, it confirmed that an important part of gB_{MG} *N*-glycans, but not all, was deglycosylated *in vivo* by EndoT.

While full-length gB_{HM} was observed in the CM (Figure 5d), no gB_{MG} could be detected (Figure S4b). This could be the direct result of gB deglycosylation by EndoT. Indeed, removal of *N*-glycans in the Golgi could unmask protease cleavage sites, decrease stability through conformational changes or favour aggregation by exposing hydrophobic residues. However, since *N*-glycans of endogenous proteins were also modified, we could not exclude an indirect, more global, effect such as an increase in some protease activity. The change in growth kinetics observed after *N*-glycan modification (Figure S2) could also impact gB accumulation indirectly. Although spiking of gB_{HM} in spent CM did not result in any detectable degradation, spiking of *in vitro* deglycosylated gB_{HM} in BY-2 cell CM and monitoring of the degradation profile at different time points by Western blotting would help to determine the impact of deglycosylation on gB_{MG} stability. The lack of impact of the spiking would suggest, as for gB_{HM}, that most degradation occurs intracellularly or in the apoplast.

Prior GlycoDelete-like strategies reported on a 95–100% efficiency of EndoT *in vivo* processing in HEK 293S, *A. thaliana* seeds, *P. pastoris* and *A. oryzae* (Li *et al.*, 2020; Meuris *et al.*, 2014; Piron *et al.*, 2015; Wang *et al.*, 2020). For all four studies, these efficiency rates were calculated based on the *N*-glycosylation content of one or two recombinant proteins containing one to three *N*-glycosylation sites. These EndoT processing rates were comparable to that obtained here for

human IgG2. Indeed, the CH2 *N*-glycosylation site of IgG2_{MG} was occupied at 93% on average with mono-GlcNAc (up to 98% for cell line *GnTII/FucT-KO-EndoT-IgG2* #16). However, the EndoT processing rate seemed to be highly dependent on the protein context, as illustrated by the variation in mono-GlcNAc content between the two IgG2_{MG} canonical N-sites. Indeed, the CH2 site had a processing rate of 23% (2.6% of the 11.2% *N*-glycans were mono-GlcNAc, Figure S7a). Hence, herein, we challenged these results further by assessing the EndoT deglycosylation level of an 18 *N*-glycosylation sites protein, gB (Figure 5e). We suggest that accessibility of the *N*-glycosylation site to EndoT determined the mono-GlcNAc content, in the same way as the *N*-glycan libraries of different *N*-glycosylation sites varied because they were not equally processed by glycosyltransferases in the secretory pathway. Therefore, the efficiency of the GlycoDelete-like strategy is dependent on the recombinant glycoprotein.

If the deglycosylation rate of recombinant proteins by EndoT needs to be improved, several strategies can be considered. First, if it does not affect its folding, expression of EndoT without the two propeptides might be beneficial. Indeed, it is likely that EndoT is activated via propeptide cleavage. As a result, removing the propeptides in the genetic construct would result in EndoT being active as soon as it is correctly folded, which is susceptible to increase the deglycosylation rate. Alternatively, expression of EndoH instead of EndoT could be investigated. Finally, the AtXylIT transmembrane domain that is used to target EndoT to the medial-Golgi could be replaced by the targeting domain of other glycosyltransferases like AtMNSVII or AtGMII (cis/medial-Golgi), At β 1,3-galactosyltransferase or rat sialyltransferase (trans-Golgi) to target EndoT to more up- or downstream Golgi sub-compartments (Dicker *et al.*, 2015; Schoberer and Strasser, 2011). EndoT could also be targeted to the ER using a KDEL retention signal.

In conclusion, the generation of a set of glyco-engineered BY-2 cell lines allowed for the production of tailor-made recombinant glycoproteins. With the mono-GlcNAc cell line, we produced recombinant proteins with minimal *N*-glycosylation in BY-2 cells. Production of an IgG2 and the vaccine antigen gB in wild type, xylose- and α 1,3-fucose-devoid, high mannose and mono-GlcNAc BY-2 cell lines and subsequent analysis of their *N*-glycosylation profile validated the interest and suitability of glyco-engineered BY-2 cells as a tool for molecular farming.

Experimental procedures

Binary plasmid construction

gB-encoding constructs were based on the pZP-RCS2-*nptII*-*mCherry-gBHis* plasmid used in previous studies (Smargiasso *et al.*, 2019). A few modifications were introduced to improve gB production. First, as it is not detected in extracellular protein samples, the 6xHis-tag encoding sequence was removed from the gB expression cassette. Second, to reduce the formation of rosette-like gB aggregates and hence favour monodispersed gB trimers, hydrophobic residues in both fusion loops were mutated for more hydrophilic residues. Third, to improve the yield, two gB expression cassettes were introduced into the I-SceI and I-CeuI cloning sites of pZP-RCS2 (Goderis *et al.*, 2002) and a *N. tabacum* Rb7 scaffold attachment region (SAR) genetic insulator was cloned in the PI-PspI site. Finally, the *neomycin phosphotransferase II* (*nptII*) resistance gene was replaced by *hygromycin phosphotransferase* (*hpt*).

To express the human IgG1 and IgG2 Lo-BM2 (Dehoux *et al.*, 2000), the plasmids pPZP-*nptII-hlgG1-LoBM2* and pPZP-*nptII-hlgG2-LoBM2* described in De Muynck *et al.* (2009) and Magy *et al.* (2014) were used to transform WT and *XylIT/FucT*-KO cell lines via *A. tumefaciens*. To transform *GnTI(FucT)*-KO cell lines, *nptII* was replaced by *hpt* resistance.

EndoT from *H. jecorina* (UniProtKB-C4RA89), without the 17 first amino acids encoding the endogenous signal sequence, was codon optimized for *A. thaliana*, fused at 5' to the sequence encoding the first 32 amino acids of AtXylIT and at 3' to the sequence encoding a FLAG-tag (DYKDDDDK) and synthesized (Genscript). *EndoT-Venus* chimeric gene was obtained by fusing *AtXylIT-EndoT* to *Venus* cDNA at 3', instead of the FLAG-tag. *AtXylIT-EndoT* and *AtXylIT-EndoT-Venus* were placed under the control of the enhanced *CaMV 35S* promoter (*En2p35S*) and the nopaline synthase terminator (*Tnos*). Then, *AtXylIT-EndoT* was cloned in the *PI-PspI* site of pPZP-*hpt-hlgG2-LoBM2* and pPZP-*hpt-mCherry-gB*. *AtXylIT-EndoT-Venus* was cloned in the *PI-PspI* site of pPZP-*nptII-mCherry-gB*.

Nicotiana tabacum BY-2 cell culture and transformation

BY-2 cells were grown as described in Herman *et al.* (2021). D11b cultures (Vasilev *et al.*, 2013) were grown for 10 days in 50 mL of medium without cyclodextrin, in 250 mL Erlenmeyer flasks.

Agrobacterium tumefaciens LBA4404VirG-mediated stable transformation of BY-2 cells was carried out as described by Navarre and Chaumont (2022). *nptII* resistance marker was used to transform WT and *XylIT/FucT*-KO BY-2 cell lines, *hpt* resistance gene was used to transform *GnTI*-KO and *GnTI/FucT*-KO (*GnTI(FucT)*-KO) cell lines. Selection of transformed cell lines was carried out on MS-agar plates containing 100 µg/mL kanamycin or 50 µg/mL hygromycin, respectively.

Light microscopy

Cell samples were imaged with a 34-channel Zeiss LSM 710 AxioObserver confocal microscope equipped with a Airyscan superresolution system and with a Plan Apochromat 25× numerical aperture 0.8 water immersion objective.

SDS-PAGE and Western blotting analysis of proteins

CM and TSCP samples were obtained as described by Herman *et al.* (2021). TCP correspond to samples collected before the final ultracentrifugation step. Microsomal fractions were obtained by resuspension of the ultracentrifugation pellet in 50 µL buffer [3 mM KH₂PO₄, 330 mM sucrose, 3 mM KCl, pH 7.8 (KOH)].

CM (µL) or TCP/TSCP/microsomal fractions (µg) were analysed by SDS-PAGE (reducing, 4–20% polyacrylamide if not stated otherwise) after denaturation (5 min at 100 °C for CM and TSCP; 15 min at 56 °C for TCP and microsomal fractions). Gels were stained with Coomassie Brilliant Blue G-250 (SERVA, 17524) or transferred onto a PVDF membrane (1704 156; Bio-Rad, Hercules, CA, USA) for Western blotting. The PVDF membrane was incubated with rabbit polyclonal antibody against EndoT (1/5000, Meuris *et al.* (2014)) or rabbit monoclonal antibody against HCMV gB (10 202-R038, 1/2000; Sino Biologicals, Beijing, China) followed by anti-rabbit polyclonal antibodies HRP-coupled (LO-RG-1-HRP, 1/10 000; SynAbs, Charleroi, Belgium) or alkaline phosphatase (AP)-coupled (A3687, 1/10 000; Sigma-Aldrich, Saint-Louis, MO, USA). Alternatively, the PVDF membrane was incubated with polyclonal antibodies against human IgG (Fc-

specific) coupled to HRP (A0170, 1/5000; Sigma-Aldrich) or Concanavalin A coupled to HRP (L6397, 1/200; Sigma-Aldrich).

Western blots using HRP-conjugated antibodies (or lectin) were revealed with BM Chemiluminescence Blotting Substrate (11 500 694 001; Roche, Basel, Switzerland). Western blots using AP-conjugated antibodies were revealed with Immuno-Star AP chemiluminescent substrate (1 705 018; Bio-Rad) or BM Purple AP substrate, precipitating (11 442 074 001; Roche). Chemiluminescence was detected using the Amersham™ Imager 600 (GE Healthcare, Chicago, IL, USA). The relative intensity of immunoblot signals was quantified with Amersham Imager 600 Analysis Software.

BY-2 cell culture growth kinetics

Three independent transgenic cell lines from each cell type were inoculated at 0.015 g/mL in 50 mL MS medium in a 250 mL Erlenmeyer flask. At each time point, 2 mL of culture were filtered on four layers of Miracloth (475 855; Calbiochem, San Diego, CA, USA) and the cell pack fresh weight was measured after centrifugation for 3 min at 2700 g.

Purification of IgG

IgG purification was carried out as described by Mercx *et al.* (2017), from 10-day-old D11b cultures.

ELISAs

IgG Lo-BM2 and gB ELISAs were respectively carried out as described in Magy *et al.* (2014) and Smargiasso *et al.* (2019).

Size exclusion chromatography

Purified IgG2 proteins (300 µL) were loaded on a Superdex 200 10/300 GL size-exclusion chromatography column (GE Healthcare) linked to the ÄKTA Prime system. The column was pre-equilibrated with 50 mM NaH₂PO₄ (pH 7.5), 150 mM NaCl, and 10% (w/v) glycerol. The elution was carried out at 0.3 mL/min, and the absorbance at 280 nm was recorded.

Mass spectrometry analysis

Total N-glycans of the secreted proteins

The determination of the N-glycan library was performed using the procedure described by Herman *et al.* (2021), with minor modifications. The PNGase F-released N-glycans and the 2-AB-labelled N-glycans were loaded on GlycoClean H and S cartridge (GKI-4025 and GKI-4726; Agilent Technologies, Santa Clara, CA, USA), respectively. The dual ESI/MALDI source solarix xR 9.4 T FT-ICR (Bruker Daltonics, Billerica, MA, USA) operating in MALDI positive ionization mode was mass calibrated using a dried spot of red phosphorus in acetone and the 2-AB labelled N-glycans obtained from bovine ribonuclease B, offering sub ppm mass accuracy. Mass range was set from 150 to 3500 and the resolving mass power was around 300 000 in the m/z region of the 2-AB labelled N-glycans.

Site-specific IgG N-glycosylation

The IgG samples were desalted using Amicon 3 kDa (Millipore, Burlington, MA, USA). The proteins were recovered in ammonium carbonate buffer 50 mM pH 7.5. Protein content was assessed using the RC DC protein assay kit (500-0019; Bio-Rad) against bovine serum albumin fraction V (BSAV-RO; Sigma-Aldrich) as standard using the recommended manufacturer procedure.

Multi-enzymatic limited digestion (MELD) on RNase B and *N. tabacum* samples was then performed (Morsa et al., 2019).

Simultaneously, to ensure correct identification of glycopeptides, a fraction of some samples (*GnTI-KO-IgG2* #25, *GnTI-KO-EndoT-IgG2* #9 and RNase B) was deglycosylated according to the procedure described by Smargiasso et al. (2019) and Herman et al. (2021). These fractions were then submitted to the MELD followed by LC–MS. The absence of glycopeptides was checked as well as the presence of Asp instead of Asn in the identified *N*-glycosylation sites, especially to confirm the non-consensus TVSWN*SGAL site. Persistence of the PNGase-resistant mono-GlcNAc after deglycosylation was confirmed.

The MELD proteolysis products were reconstituted at 15 pmol in 9 μ L water +0.1% trifluoroacetic acid. M-Class nanoUPLC pump (Waters, Milford, MA, USA) was used for the separation of (glyco)peptides by reverse phase liquid chromatography (LC). The LC and the MS methods used were those described by Morsa et al. (2019), with minor modifications. The LC flow rate was set at 0.5 μ L/min. The MS system was a Q-Exactive quadrupole-Orbitrap instrument (ThermoFisher Scientific, Waltham, MA, USA) using NCE = 27 (normalized collision energy).

The raw LC–MS/MS data were submitted to PEAK X pro for analysis (Method S1).

Differential scanning fluorimetry

DSF was carried out based on the protocol described by Moggridge et al. (2017). Briefly, purified IgG samples were diluted twice in phosphate buffered saline (100 mM phosphate, 150 mM NaCl, pH 7.0) containing SYPRO Orange Protein Gel Stain (S6650; Invitrogen, Waltham, MA, USA). Samples were transferred into a MicroAmp™ Optical 96-Well Reaction Plate (N8010560; Applied Biosystems, Waltham, MA, USA). Each sample was run as a technical triplicate and successive dilutions were performed. DSF measurements were performed using a temperature increase from 15 °C to 90 °C with a ramp of 1 °C/min (StepOnePlus™ Real-Time PCR System; Applied Biosystems). Mean melting temperatures were calculated as the temperature corresponding to the maximum value of the mean derivative curves. Mean derivative curves were obtained as the first derivative of the mean melt curves. For graphing, the raw data were normalized (maximal value = 100%).

In vitro deglycosylation assay

Twenty micrograms of TSCP or 20 μ L of CM were denatured by heating for 10 min at 100 °C in the manufacturer's glycoprotein denaturing buffer, to ensure optimal *N*-site accessibility. Samples were then incubated for 1 h at 37 °C with EndoH 50 U (P0703; New England Biolabs, Ipswich, MA, USA) or PNGase F 25 U (P0704; New England Biolabs) using the manufacturer's conditions. Control samples were run in parallel but without the EndoH and PNGase F enzymes. Samples were then visualized by Western blotting.

Acknowledgements

We acknowledge Nicolas Bailly (UCLouvain) for the optimization of the gB nucleotide sequence, Adeline Courtoy (UCLouvain), Joseph Nader (UCLouvain) and Marie-Eve Renard (UCLouvain) for their technical assistance as well as Prof. Marc Boutry for fruitful discussions and critical reading of the manuscript. We also thank Dr. Leander Meuris (UGent) for providing anti-EndoT antibodies. Special thanks to the IMAB platform (UCLouvain) and the GIGA

proteomics facility (ULiège) for the technical assistance and providing access to the UPLC and the Q-Exactive instruments. This work was supported by a grant from the Service Public de Wallonie SPW DGO6 in Belgium (WALLInnov-GlycoCell-1810010). XH is a recipient of a fellowship from the Fonds pour la Formation à la Recherche dans l'Industrie et l'Agriculture (Belgium). MP is a recipient of a fellowship from the Fonds de la Recherche Scientifique (Belgium). The mass spectrometry laboratory is supported by the European Union's Horizon 2020 Research and Innovation Program under grant agreement No. 731077 (EU FT-ICR MS project, INFRAIA-02-2017) and from the European Union and Wallonia program FEDER BIOMED HUB Technology Support (No. 2.2.1/996) for the funding of the Solarix XR 9.4T. Software development is also supported by the European Union's Horizon 2020 program (EURLipids Interreg Eurogio Meuse-Rhine). The UPLC and the Q-Exactive were financed by the FEDER and Wallonia Region.

Conflict of interest statement

The authors declare that the research was conducted in the absence of any commercial or financial relationships that could be construed as a potential conflict of interest.

Author contributions

XH, CN and FC: conceptualization. XH and JF: methodology. XH, JF, MP and CN: investigation. XH, JF, and CN: data curation. XH: writing – original draft preparation. CN, JF and FC: writing – review and editing. CN, LQ and FC: supervision and funding acquisition. All authors have read and agreed to the manuscript.

Data availability statement

The MS raw data are available on request (loic.quinton@uliege.be or johann.far@uliege.be).

References

- Akazawa-Ogawa, Y., Nagai, H. and Hagihara, Y. (2018) Heat denaturation of the antibody, a multi-domain protein. *Biophys. Rev.* **10**, 255–258.
- Čaval, T., Heck, A.J.R. and Reiding, K.R. (2021) Meta-heterogeneity: evaluating and describing the diversity in glycosylation between sites on the same glycoprotein. *Mol Cell Proteomics* **20**, 100010.
- Chen, J.R., Yu, Y.H., Tseng, Y.C., Chiang, W.L., Chiang, M.F., Ko, Y.A., Chiu, Y.K. et al. (2014a) Vaccination of monoglycosylated hemagglutinin induces cross-strain protection against influenza virus infections. *Proc. Natl. Acad. Sci. USA* **111**, 2476–2481.
- Chen, W.H., Du, L., Chag, S.M., Ma, C., Tricoche, N., Tao, X., Seid, C.A. et al. (2014b) Yeast-expressed recombinant protein of the receptor-binding domain in SARS-CoV spike protein with deglycosylated forms as a SARS vaccine candidate. *Hum. Vaccin. Immunother.* **10**, 648–658.
- De Muynck, B., Navarre, C., Nizet, Y., Stadlmann, J. and Boutry, M. (2009) Different subcellular localization and glycosylation for a functional antibody expressed in *Nicotiana tabacum* plants and suspension cells. *Transgenic Res.* **18**, 467–482.
- Dehoux, J.P., Hori, S., Talpe, S., Bazin, H., Latinne, D., Soares, M.P. and Gianello, P. (2000) Specific depletion of preformed IgM natural antibodies by administration of anti- μ monoclonal antibody suppresses hyperacute rejection of pig to baboon renal xenografts. *Transplantation* **70**, 935–946.
- Dicker, M., Schoberer, J., Vavra, U. and Strasser, R. (2015) Subcellular targeting of proteins involved in modification of plant *N*- and *O*-glycosylation. In *Glyco-Engineering*, pp. 249–267. New York, NY: Humana Press.

- Fanata, W.I.D., Lee, K.H., Son, B.H., Yoo, J.Y., Harmoko, R., Ko, K.S., Ramasamy, N.K. *et al.* (2013) N-glycan maturation is crucial for cytokinin-mediated development and cellulose synthesis in *Oryza sativa*. *Plant J.* **73**, 966–979.
- Fox, J.L. (2012) First plant-made biologic approved. *Nat. Biotechnol.* **30**, 472–473.
- Fujiyama, K., Furukawa, A., Katsura, A., Misaki, R., Omasa, T. and Seki, T. (2007) Production of mouse monoclonal antibody with galactose-extended sugar chain by suspension cultured tobacco BY2 cells expressing human β (1, 4)-galactosyltransferase. *Biochem. Biophys. Res. Commun.* **358**, 85–91.
- Goderis, I.J.W.M., De Bolle, M.F.C., Francois, I.E.J.A., Wouters, P.F.J., Broekaert, W.F. and Cammue, B.P.A. (2002) A set of modular plant transformation vectors allowing flexible insertion of up to six expression units. *Plant Mol. Biol.* **50**, 17–27.
- Hanania, U., Ariel, T., Tekoah, Y., Fux, L., Sheva, M., Gubbay, Y., Weiss, M. *et al.* (2017) Establishment of a tobacco BY2 cell line devoid of plant-specific xylose and fucose as a platform for the production of biotherapeutic proteins. *Plant Biotechnol. J.* **15**, 1120–1129.
- Herman, X., Far, J., Courtoy, A., Bouhon, L., Quinton, L., De Pauw, E., Chaumont, F. *et al.* (2021) Inactivation of N-acetylglucosaminyltransferase I and α 1,3-fucosyltransferase genes in *N. tabacum* BY-2 cells results in glycoproteins with highly homogeneous, high-mannose N-glycans. *Front. Plant Sci.* **12**, 634023.
- Huang, H.Y., Liao, H.Y., Chen, X., Wang, S.W., Cheng, C.W., Shahed-Al-Mahmud, M., Liu, Y.M. *et al.* (2022) Vaccination with SARS-CoV-2 spike protein lacking glycan shields elicits enhanced protective responses in animal models. *Sci. Transl. Med.* **14**, eabm0899.
- Ju, M.S. and Jung, S.T. (2014) Aglycosylated full-length IgG antibodies: steps toward next-generation immunotherapeutics. *Curr. Opin. Biotechnol.* **30**, 128–139.
- Kajiura, H., Misaki, R., Fujiyama, K. and Seki, T. (2011) Stable coexpression of two human sialylation enzymes in plant suspension-cultured tobacco cells. *J. Biosci. Bioeng.* **111**, 471–477.
- Kang, C.E., Lee, S., Ahn, T., Seo, D.H., Ko, B.J., Jung, M., Lee, J. *et al.* (2022) Antibody-dependent cellular cytotoxicity-null effector developed using mammalian and plant GlycoDelete platform. *Sci. Rep.* **12**, 19030.
- Karg, S.R., Frey, A.D. and Kallio, P.T. (2010) Reduction of N-linked xylose and fucose by expression of rat β 1, 4-N-acetylglucosaminyltransferase III in tobacco BY-2 cells depends on Golgi enzyme localization domain and genetic elements used for expression. *J. Biotechnol.* **146**, 54–65.
- Kasturi, L., Eshleman, J.R., Wunner, W.H. and Shakin-Eshleman, S.H. (1995) The hydroxy amino acid in an Asn-X-Ser/Thr Sequon can influence N-linked core glycosylation efficiency and the level of expression of a cell surface glycoprotein. *J. Biol. Chem.* **270**, 14756–14761.
- Kaufm st-Soboll, H., Mertens-Beer, M., Brehler, R., Albert, M. and von Schaeuwen, A. (2021) Complex N-glycans are important for normal fruit ripening and seed development in tomato. *Front. Plant Sci.* **12**, 635962.
- Kiyoshi, M., Tsumoto, K., Ishii-Watabe, A. and Caaveiro, J.M. (2017) Glycosylation of IgG-Fc: a molecular perspective. *Int. Immunol.* **29**, 311–317.
- Lee, N.E., Kim, S.H., Yu, D.Y., Woo, E.J., Kim, M.I., Seong, G.S., Lee, S.M. *et al.* (2020) Aglycosylated antibody-producing mice for aglycosylated antibody-lectin coupled immunoassay for the quantification of tumor markers (ALIQAT). *Commun. Biol.* **3**, 636.
- Li, Q., Higuchi, Y., Tanabe, K., Katakura, Y. and Takegawa, K. (2020) Secretory production of N-glycan-deleted glycoprotein in *Aspergillus oryzae*. *J. Biosci. Bioeng.* **129**, 573–580.
- Magy, B., Tollet, J., Laterre, R., Boutry, M. and Navarre, C. (2014) Accumulation of secreted antibodies in plant cell cultures varies according to the isotype, host species and culture conditions. *Plant Biotechnol. J.* **12**, 457–467.
- Mamedov, T., Ghosh, A., Jones, R.M., Mett, V., Farrance, C.E., Musiyuchuk, K., Horsey, A. *et al.* (2012) Production of non-glycosylated recombinant proteins in *Nicotiana benthamiana* plants by co-expressing bacterial PNGase F. *Plant Biotechnol. J.* **10**, 773–782.
- Mamedov, T., Cicek, K., Gulec, B., Ungor, R. and Hasanova, G. (2017) *In vivo* production of non-glycosylated recombinant proteins in *Nicotiana benthamiana* plants by co-expression with Endo- β -N-acetylglucosaminidase H (Endo H) of *Streptomyces pilicatus*. *PLoS One* **12**, e0183589.
- Mamedov, T., Yuksel, D., Ilgin, M., Gurbuzaslan, I., Gulec, B., Yetiskin, H., Uygut, M.A. *et al.* (2021) Plant-produced glycosylated and *In vivo* Deglycosylated receptor binding domain proteins of SARS-CoV-2 induce potent neutralizing responses in mice. *Viruses* **13**, 1595.
- Mercx, S., Smargiasso, N., Chaumont, F., De Pauw, E., Boutry, M. and Navarre, C. (2017) Inactivation of the β (1,2)-xylosyltransferase and the α (1,3)-fucosyltransferase genes in *Nicotiana tabacum* BY-2 cells by a multiplex CRISPR/Cas9 strategy results in glycoproteins without plant-specific glycans. *Front. Plant Sci.* **8**, 403.
- Meuris, L., Santens, F., Elson, G., Festjens, N., Boone, M., Dos Santos, A., Devos, S. *et al.* (2014) GlycoDelete engineering of mammalian cells simplifies N-glycosylation of recombinant proteins. *Nat. Biotechnol.* **32**, 485–489.
- Misaki, R., Kimura, Y., Palacpac, N.Q., Yoshida, S., Fujiyama, K. and Seki, T. (2003) Plant cultured cells expressing human β 1, 4-galactosyltransferase secrete glycoproteins with galactose-extended N-linked glycans. *Glycobiology* **13**, 199–205.
- Misaki, R., Fujiyama, K. and Seki, T. (2006) Expression of human CMP-N-acetylneuraminic acid synthetase and CMP-sialic acid transporter in tobacco suspension-cultured cell. *Biochem. Biophys. Res. Commun.* **339**, 1184–1189.
- Moggridge, J., Biggar, K., Dawson, N. and Storey, K.B. (2017) Sensitive detection of immunoglobulin G stability using in real-time isothermal differential scanning Fluorimetry: Determinants of protein stability for antibody-based therapeutics. *Technol. Cancer Res. Treat.* **16**, 997–1005.
- Morsa, D., Baiwir, D., La Rocca, R., Zimmerman, T.A., Hanozin, E., Grifn e, E., Longuesp e, R. *et al.* (2019) Multi-enzymatic limited digestion: the next-generation sequencing for proteomics? *J. Proteome Res.* **18**, 2501–2513.
- Nagashima, Y., von Schaeuwen, A. and Koiva, H. (2018) Function of N-glycosylation in plants. *Plant Sci.* **274**, 70–79.
- Nandakumar, K.S., Collin, M., Happonen, K.E., Croxford, A.M., Lundstr m, S.L., Zubarev, R.A., Rowley, M.J. *et al.* (2013) Dominant suppression of inflammation by glycan-hydrolyzed IgG. *Proc. Natl. Acad. Sci. USA* **110**, 10252–10257.
- Navarre, C. and Chaumont, F. (2022) Production of recombinant glycoproteins in *Nicotiana tabacum* BY-2 suspension cells. *Methods Mol. Biol.* **2480**, 81–88.
- Navarre, C., Smargiasso, N., Duvivier, L., Nader, J., Far, J., De Pauw, E. and Boutry, M. (2017) N-Glycosylation of an IgG antibody secreted by *Nicotiana tabacum* BY-2 cells can be modulated through co-expression of human β -1, 4-galactosyltransferase. *Transgenic Res.* **26**, 375–384.
- Paccalet, T., Bardor, M., Rihouey, C., Delmas, F., Chevalier, C., D’Aoust, M.A., Faye, L. *et al.* (2007) Engineering of a sialic acid synthesis pathway in transgenic plants by expression of bacterial Neu5Ac-synthesizing enzymes. *Plant Biotechnol. J.* **5**, 16–25.
- Palacpac, N.Q., Yoshida, S., Sakai, H., Kimura, Y., Fujiyama, K., Yoshida, T. and Seki, T. (1999) Stable expression of human β 1, 4-galactosyltransferase in plant cells modifies N-linked glycosylation patterns. *Proc. Natl. Acad. Sci. USA* **96**, 4692–4697.
- Piron, R., Santens, F., De Paepe, A., Depicker, A. and Callewaert, N. (2015) Using GlycoDelete to produce proteins lacking plant-specific N-glycan modification in seeds. *Nat. Biotechnol.* **33**, 1135–1137.
- Planinc, A., Dejaegher, B., Vander Heyden, Y., Viaene, J., Van Praet, S., Rappez, F., Van Antwerpen, P. *et al.* (2017) Batch-to-batch N-glycosylation study of infliximab, trastuzumab and bevacizumab, and stability study of bevacizumab. *Eur. J. Hosp. Pharm.* **24**, 286–292.
- Schleiss, M.R., Permar, S.R. and Plotkin, S.A. (2017) Progress toward development of a vaccine against congenital cytomegalovirus infection. *Clin. Vaccine Immunol.* **24**, e00268–e00217.
- Schoberer, J. and Strasser, R. (2011) Sub-compartmental organization of Golgi-resident N-glycan processing enzymes in plants. *Mol. Plant* **4**, 220–228.
- Smargiasso, N., Nader, J., Rioux, S., Mazzucchelli, G., Boutry, M., De Pauw, E., Chaumont, F. *et al.* (2019) Exploring the N-glycosylation profile of glycoprotein B from human cytomegalovirus expressed in CHO and *Nicotiana tabacum* BY-2 cells. *Int. J. Mol. Sci.* **20**, 3741.
- Strasser, R. (2022) Recent developments in deciphering the biological role of plant complex N-glycans. *Front. Plant Sci.* **13**, 897549.
- Valliere-Douglass, J.F., Kodama, P., Mujacic, M., Brady, L.J., Wang, W., Wallace, A., Yan, B. *et al.* (2009) Asparagine-linked oligosaccharides present

- on a non-consensus amino acid sequence in the CH1 domain of human antibodies. *J. Biol. Chem.* **284**, 32493–32506.
- Valliere-Douglass, J.F., Eakin, C.M., Wallace, A., Ketchum, R.R., Wang, W., Treuheit, M.J. and Balland, A. (2010) Glutamine-linked and non-consensus asparagine-linked oligosaccharides present in human recombinant antibodies define novel protein glycosylation motifs. *J. Biol. Chem.* **285**, 16012–16022.
- Van Landuyt, L., Lonigro, C., Meuris, L. and Callewaert, N. (2019) Customized protein glycosylation to improve biopharmaceutical function and targeting. *Curr. Opin. Biotechnol.* **60**, 17–28.
- Vasilev, N., Grömping, U., Lipperts, A., Raven, N., Fischer, R. and Schillberg, S. (2013) Optimization of BY-2 cell suspension culture medium for the production of a human antibody using a combination of fractional factorial designs and the response surface method. *Plant Biotechnol. J.* **11**, 867–874.
- Wada, R., Matsui, M. and Kawasaki, N. (2019) Influence of *N*-glycosylation on effector functions and thermal stability of glycoengineered IgG1 monoclonal antibody with homogeneous glycoforms. *MAbs* **11**, 350–372.
- Wang, C.C., Chen, J.R., Tseng, Y.C., Hsu, C.H., Hung, Y.F., Chen, S.W., Chen, C.M. et al. (2009) Glycans on influenza hemagglutinin affect receptor binding and immune response. *Proc. Natl. Acad. Sci. USA* **106**, 18137–18142.
- Wang, S., Rong, Y., Wang, Y., Kong, D., Wang, P.G., Chen, M. and Kong, Y. (2020) Homogeneous production and characterization of recombinant *N*-GlcNAc-protein in *Pichia pastoris*. *Microb. Cell Factories* **19**, 1–11.
- Wu, C.Y., Cheng, C.W., Kung, C.C., Liao, K.S., Jan, J.T., Ma, C. and Wong, C.H. (2022) Glycosite-deleted mRNA of SARS-CoV-2 spike protein as a broad-spectrum vaccine. *Proc. Natl. Acad. Sci. USA* **119**, e2119995119.
- Yin, B.J., Gao, T.N.Y., Li, Y., Tang, S.Y., Liang, L.M. and Xie, Q. (2011) Generation of glyco-engineered BY2 cell lines with decreased expression of plant-specific glycoepitopes. *Protein Cell* **2**, 41–47.
- Zheng, K., Bantog, C. and Bayer, R. (2011) The impact of glycosylation on monoclonal antibody conformation and stability. *MAbs* **3**, 568–576.

Supporting information

Additional supporting information may be found online in the Supporting Information section at the end of the article.

Figure S1 Relative amounts of total *N*-glycans from secreted glycoproteins of *GnTI*-KO and *GnTII/FucT*-KO cell lines.

Figure S2 Growth kinetics of WT, *GnTII(FucT)*-KO and *GnTII/FucT*-KO-*EndoT* cell lines.

Figure S3 *EndoT* content of *GnTI*-KO-*EndoT*-IgG2 and *GnTII/FucT*-KO-*EndoT*-IgG2 cell lines.

Figure S4 Kinetics of accumulation of recombinant glycoproteins in the culture medium of glyco-engineered BY-2 cell lines.

Figure S5 Deglycosylation gel shift assay of secreted recombinant glycovariants

Figure S6 Purification of IgG2 from BY-2 cell cultures.

Figure S7 Relative amount of *N*-glycans on the N-site CVRPN*YSGF (a) and TVSWN*SGAL (b) of secreted IgG2.

Figure S8 Relative amount of *N*-glycans on the *N*-sites of secreted IgG2, per type of cell line.

Figure S9 Analysis of IgG thermal stability by differential scanning fluorimetry.

Figure S10 Thermal stability of old and new IgG2_{FG} and IgG2_{ΔX/ΔF}.

Figure S11 Spiking of gB_{HM} in BY-2 cell culture medium

Table S1 Summary of glycoengineered BY-2 cell lines, *N*-glycans and glycovariants nomenclature

Table S2 Recombinant glycoprotein concentration in the culture medium

Table S3 Relative amount of *N*-glycans on the *N*-sites of secreted IgG2

Table S4 Custom plant *N*-glycan exact mass table used for the data processing with PEAKS Xpro.

Method S1 LC-MS/MS raw data analysis.

Movie S1 Localization of AtXylT-*EndoT*.